Journal of Power Sources 216 (2012) 368–375

Contents lists available at SciVerse ScienceDirect

Journal of Power Sources

journal homepage: www.elsevier.com/locate/jpowsour

Structural, electrochemical and thermal stability investigations on $LiNi_{0.5-x}Al_{2x}Mn_{1.5-x}O_4$ ($0 \leq 2x \leq 1.0$) as 5 V cathode materials

G.B. Zhong [a], Y.Y. Wang [a], X.J. Zhao [b], Q.S. Wang [b], Y. Yu [a], C.H. Chen [a,*]

[a] CAS Key Laboratory of Materials for Energy Conversion, Department of Materials Science and Engineering, University of Science and Technology of China, Anhui, Hefei 230026, PR China

[b] State Key Laboratory of Fire Science, University of Science and Technology of China, Anhui, Hefei 230026, PR China

HIGHLIGHTS

- Al-doped compounds $LiNi_{0.5-x}Al_{2x}Mn_{1.5-x}O_4$ ($0 \leq 2x \leq 1.0$) with a wide doping range are prepared and characterized.
- The optimal Al concentration in the $LiNi_{0.5-x}Al_{2x}Mn_{1.5-x}O_4$ is $0.05 \leq 2x \leq 0.10$.
- The thermal stability of $LiNi_{0.5-x}Al_{2x}Mn_{1.5-x}O_4$ electrodes before 225 °C is effectively improved by Al-doping.

ARTICLE INFO

Article history:
Received 23 March 2012
Received in revised form
7 May 2012
Accepted 28 May 2012
Available online 6 June 2012

Keywords:
Lithium-ion batteries
Spinel
Aluminum doping
Lithium nickel manganese oxide
Thermal stability

ABSTRACT

A series of Al-substituted spinel powders $LiNi_{0.5-x}Al_{2x}Mn_{1.5-x}O_4$ ($0 \leq 2x \leq 1.0$) have been prepared and the effects of Al concentration on the structural, electrochemical and thermal properties are investigated. The XRD patterns show that impurity arises when $2x \geq 0.6$. The FTIR and Raman spectra indicate that the introduction of Al in the $LiNi_{0.5}Mn_{1.5}O_4$ increases the disordering degree of Ni/Mn ions, changing the spinel structure from $P4_332$ to $Fd\bar{3}m$. Cyclic voltammetry tests show that the voltage step between Ni^{2+}/Ni^{3+} and Ni^{3+}/Ni^{4+} have a sudden leap at $2x = 0.075$, responding to the structural difference of the spinels. The Al concentration is optimized in the range of $0.05 \leq 2x \leq 0.1$, in which the cyclic stability and rate capability of the $LiNi_{0.5-x}Al_{2x}Mn_{1.5-x}O_4$ spinels are significantly improved. At room temperature the $LiNi_{0.45}Al_{0.10}Mn_{1.45}O_4$ presents the best cycle performance with the capacity retention of 95.4% after 500 cycles at 1C rate, and the best rate capability with the discharge capacity of 119 mAh g^{-1} at 10C rate, which is about 93.7% of its capacity at 0.5C. The thermal properties of the spinels have been tested by C80 calorimeter and the results show that introduction of Al in $LiNi_{0.5}Mn_{1.5}O_4$ can effectively suppress the exothermic reaction below 225 °C, thus improve the safety of the high voltage cathode material.

1. Introduction

Lithium ion batteries have been widely used in portable electronic products in the past decade. However, they fall short of meeting the demands dictated by powering of both hybrid electric vehicles (HEVs) and electric vehicles (EVs) or by the large-scale storage systems of renewable energies (wind, solar). The EV applications require high energy-density batteries that enable a reasonable driving range after each charge and maintain acceptable speeds. Even in the traditional mobile phone market, current lithium ion batteries can not match the development of smart mobile phones, which request higher energy density than ever before. The energy density of a battery is the product of its capacity and its potential, and is mainly governed by the positive electrode. In this regard, $LiNi_{0.5}Mn_{1.5}O_4$ is one of the most promising cathode materials for next generation lithium ion batteries, because it has high operating potential (4.7 V vs. lithium) and three-dimensional lithium ion diffusion paths in the spinel lattice [1–3]. The energy density calculated based on the mass of cathode materials of $LiNi_{0.5}Mn_{1.5}O_4$ is about 30% higher than that of $LiMn_2O_4$ and $LiFePO_4$ [4]. Therefore, lithium ion batteries with $LiNi_{0.5}Mn_{1.5}O_4$-based positive electrodes are expected to provide higher power/energy density.

Safety concern is one of the most important issues for the development of lithium ion batteries, especially for large-size applications in EV and HEV [5,6]. Xiang et al. have investigated the thermal stability of the electrolyte in contact with various delithiated cathodes (Li_xCoO_2, $Li_xNi_{0.8}Co_{0.15}Al_{0.05}O_2$, $Li_xNi_{1/3}Co_{1/3}Mn_{1/3}O_2$, $Li_xMn_2O_4$, $Li_xNi_{0.5}Mn_{0.5}O_2$, $Li_xNi_{0.5}Mn_{1.5}O_4$ and Li_xFePO_4) [7]. They have found that the 5 V cathode material $LiNi_{0.5}Mn_{1.5}O_4$ has the worst thermal stability. Two distinct exothermic peaks are

* Corresponding author. Tel.: +86 551 3606971; fax: +86 551 3601592.
E-mail address: cchchen@ustc.edu.cn (C.H. Chen).

0378-7753/$ – see front matter © 2012 Elsevier B.V. All rights reserved.
http://dx.doi.org/10.1016/j.jpowsour.2012.05.108

observed at around 106 °C and 150 °C for this Mn-based spinel. Much effort has been devoted to alleviate the safety issue, such as adding nonflammable addictive [8–13] and using ionic liquid electrolytes [14–17]. However, the extra safety is usually achieved at the expense of the battery performance or cost. Thus, the priority consideration should be put to prevent the appearance of thermal runaway induced by the exothermal reactions between the cathode materials and electrolyte.

In recent years, studies on $LiNi_{0.5}Mn_{1.5}O_4$ have been predominantly focused on the improvement in its electrochemical performance using various methods, such as lattice doping with Ru [18], Cr [19,20], Zn [21] and Fe [22]; surface modification with ZnO [23,24], Al_2O_3 [25] and Bi_2O_3 [26]; and syntheses of nanoparticle materials [3,27,28]. However, the thermal stability of the $LiNi_{0.5}Mn_{1.5}O_4$ in the electrolyte is usually ignored. In our previous work, we have investigated the effects of Al substitution for Ni or Mn in $LiNi_{0.5}Mn_{1.5}O_4$ spinel on the structures and electrochemical properties [4]. Nevertheless, the Al content was not optimized and the thermal stability of these Al-doped spinels was not examined then. In this work, a series of spinels $LiNi_{0.5-x}Al_{2x}Mn_{1.5-x}O_4$ with different amount of Al ($0 \leq x \leq 1.0$) are prepared; their electrochemical performances at different current densities and temperatures are examined and compared to obtain an optimized range of Al content. Moreover, their thermal stabilities in commercial electrolyte are also investigated to have an evaluation on the cell safety.

2. Experimental

First, $LiNi_{0.5-x}Al_{2x}Mn_{1.5-x}O_4$ ($2x = 0$, 0.025, 0.05, 0.075, 0.1, 0.2, 0.6, 1) samples were synthesized by a thermopolymerization method [4]. Stoichiometric amounts of $LiNO_3$ (5% excess), $Ni(NO_3)_2 \cdot 6H_2O$, $Al(NO_3)_3 \cdot 9H_2O$ and $Mn(CH_3COO)_2 \cdot 4H_2O$ were dissolved in deionized water to obtain aqueous solutions (0.2 M). Then acrylic acid (AA) was added into the solutions with AA–H_2O (1:2, v/v) as mixed solvents. The solutions were heated at 150 °C for 10 h to complete the thermopolymerization reaction. The products were first preheated at 500 °C for 10 h to get rid of poly(acrylic acid), and a subsequent heat treatment was carried out at 900 °C for 15 h followed by annealing at 700 °C for 48 h. All the heat treatment processes were carried out in air atmosphere.

The crystalline structures of the samples were characterized by X-ray diffraction (XRD) using a diffractometer (Philips X'pert Pro Super, Cu Kα radiation). The diffraction patterns were recorded at room temperature in the 2θ range from 10 to 80° with a scanning rate of 2.0° min^{-1}. The $LiNi_{0.5-x}Al_{2x}Mn_{1.5-x}O_4$ ($0 \leq 2x \leq 0.60$) samples were analyzed by Fourier-transformed infrared (FTIR) spectroscopy (TENSOR27, Bruker, Germany). The Raman spectra of the $LiNi_{0.5-x}Al_{2x}Mn_{1.5-x}O_4$ ($0 \leq 2x \leq 0.60$) samples were also measured with a Confocal Laser Micro Raman Spectrometer (LABRAM-HR, Jobin Yvon) using an excitation light of 514.5 nm from Ar ion laser (the excitation power is less than 1.0 mW). To have more reliable data, each Raman spectrum was the average of 3 scans collected at a spectral resolution of 2.0 cm^{-1}. Their particle sizes and morphology were also observed under a scanning electron microscope (JSM-6390LA, JEOL).

The electrochemical performance of each sample was evaluated with standard CR2032 coin cells $LiNi_{0.5-x}Al_{2x}Mn_{1.5-x}O_4$/Li with a polypropylene membrane (Celgard 2400) as the separator and 1 M $LiPF_6$ in ethylene carbonate (EC) − dimethyl carbonate (DMC) (1:1 w/w, Zhuhai Smoothway Electronics Materials Co., Ltd.) as the electrolyte. The cathode laminate was prepared by casting a slurry consisting of a spinel powder (80 wt.%), acetylene black (10 wt.%), and poly(vinylidene fluoride) (PVDF) (10 wt.%) dispersed in 1-methyl-2-pyrrolidinone (NMP) onto an aluminum foil with a doctor blade. The laminate was then dried at 70 °C for 10 h and punched into round discs (14 mm in diameter). The mass of active material in each disc was about 4.5–5 mg. All cells were fabricated in an argon-filled glove box (MBraun Labmaster 130).

The cyclic voltammograms (CV) of $LiNi_{0.5-x}Al_{2x}Mn_{1.5-x}O_4$/Li cells were measured on a CHI 604B electrochemical workstation from 3.5 to 5.1 V at a scan rate of 0.05 mV s^{-1}. The cells were also galvanostatically cycled on a multi-channel battery cycler (Neware BTS2300, Shenzhen) in the voltage window from 3.5 to 5.0 V. The performances at high temperature were tested at 55 °C by laying the cells in an oven.

To prepare the samples for thermal stability study, the $LiNi_{0.5-x}Al_{2x}Mn_{1.5-x}O_4$/Li cells were cycled at 0.2C and disassembled at the full charged state of 5.0 V in the third cycle. Then the positive electrodes were washed in DMC to remove the original electrolyte. After drying, the cathode materials (containing acetylene black and PVDF) were scraped from the Al current collector. 20 mg cathode materials and 50 mg electrolyte of 1 M $LiPF_6$/EC + DMC were added into a stainless steel sample tube, which was subsequently sealed for the calorimetry measurement by Setaram C80 calorimeter (Calvet). All the procedure was operated in the glove box to make sure of the argon circumstance. The calorimetric measurements were carried out at a heating rate of 0.2 °C min^{-1} from 30 °C to 300 °C. The heat flow was calculated based on the total weight of the cathode materials and the electrolyte.

3. Results and discussion

3.1. Crystalline structure and morphology

The results of X-ray diffraction analysis of the $LiNi_{0.5-x}Al_{2x}Mn_{1.5-x}O_4$ ($0 \leq 2x \leq 1.0$) powders are presented in Fig. 1. They all exhibit a pure ($x \leq 0.2$) or a main phase of the typical cubic spinel diffraction pattern (Fig. 1a). When $2x \geq 0.6$, some peaks of impurity attributed to $LiAlO_2$ are observed. All the peaks of the Al-doped samples can be indexed into the space group of $Fd\bar{3}m$ (JCPDS No. 80–2162), while the non-doped $LiNi_{0.5}Mn_{1.5}O_4$ can be indexed with a $P4_332$ symmetry due to the appearance of the weak peaks located at $2\theta = 15.3°$, 39.7°, 45.7° and 57.5°. The structural difference in these two symmetries corresponds to the disordering degree of the cations (Ni, Mn and Al) on the B-site in the spinel lattice. The symmetry of the samples will be discussed in the results of subsequent FTIR and Raman spectra. Fig. 1b shows the lattice parameters of $LiNi_{0.5-x}Al_{2x}Mn_{1.5-x}O_4$ ($0 \leq 2x \leq 1.0$) powders. It can be seen that the lattice parameter of $LiNi_{0.5-x}Al_{2x}Mn_{1.5-x}O_4$ decreases with increasing $2x$, except for the non-doped $LiNi_{0.5}Mn_{1.5}O_4$. This is because the ionic radius of Al^{3+} ($R_{Al3+} = 54$ pm) is smaller than that of $(R_{Ni2+} + R_{Mn4+})/2$ (61 pm). According to Kunduraci et al., the disordering of the B-site cations in Li$[Ni_{0.5}Mn_{1.5}]O_4$ can increase the volume of the unit cell [29]. Therefore, the lattice parameter of $LiNi_{0.4875}Al_{0.025}Mn_{1.4875}O_4$ is larger than that of $LiNi_{0.5}Mn_{1.5}O_4$ (Fig. 1b).

To distinguish more clearly the $P4_332$ structure from $Fd\bar{3}m$ structure, FTIR and Raman spectra are also used. According to Amatucci et al. [29,30], P-type and F-type can be distinguished by two methods: (1) the P-type has eight IR absorption bands while the F-type has only five; (2) the intensity ratios among the absorption signals are different in the P-type and F-type samples. For example, with increasing degree of lattice ordering, the intensity of Ni–O band at 588 cm^{-1} increases while that of Mn–O band at 619 cm^{-1} decreases. Thus, for this study, the infrared spectra of $LiNi_{0.5-x}Al_{2x}Mn_{1.5-x}O_4$ ($0 \leq 2x \leq 0.60$) are shown in Fig. 2a. It can be seen that the non-doped $LiNi_{0.5}Mn_{1.5}O_4$ has eight well-resolved absorption bands. With increasing the Al content, the intensity of these bands gradually decreases. Meanwhile, the signals at 469 and 480 cm^{-1} become overlapped, and the bands at 431 and 649 cm^{-1}

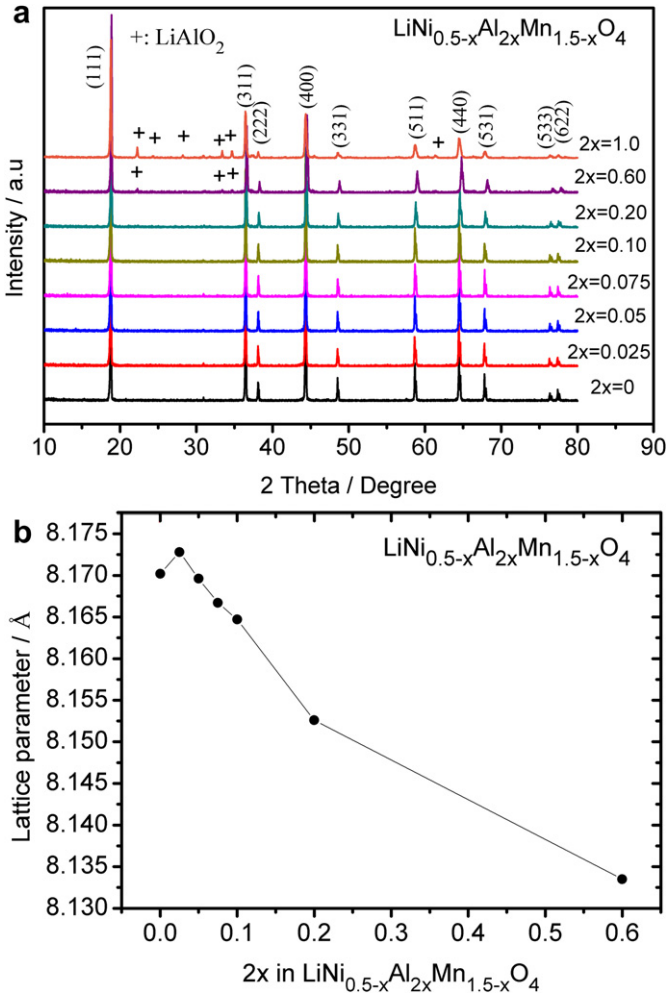

Fig. 1. (a) XRD patterns and (b) lattice parameter change of $LiNi_{0.5-x}Al_{2x}Mn_{1.5-x}O_4$ ($0 \le 2x \le 1.0$) powders.

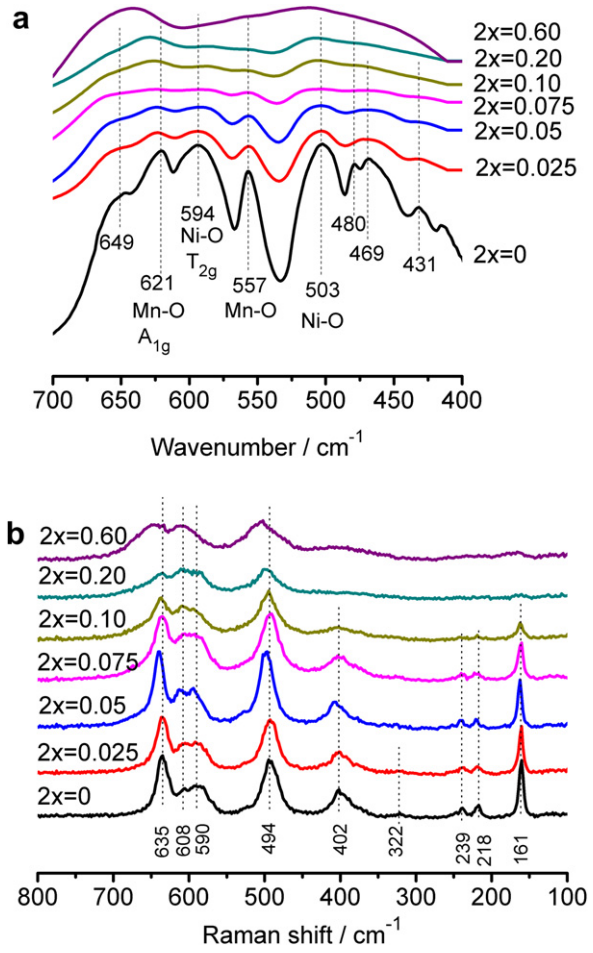

Fig. 2. (a) FTIR spectra and (b) Raman spectra of $LiNi_{0.5-x}Al_{2x}Mn_{1.5-x}O_4$ ($0 \le 2x \le 0.60$) powders.

disappear when $2x \ge 0.075$. All these results indicate that the ordering of Ni and Mn ions is destroyed by Al-doping, and the disordering degree increases with increasing Al content. The trends in Raman spectra (Fig. 2b) are consistent with infrared data. According to Oh et al. [31] and Julien [32], the strong band around 635 cm^{-1} is assigned to the symmetric Mn–O stretching mode of MnO_6 octahedra (A1g). Both peaks around 402 and 494 cm^{-1} are associated with the Ni^{2+}–O stretching mode in the structure. And the peak near 580–606 cm^{-1} is considered as $T2g^{(3)}$ of the spinel compound. The splitting of $T2g^{(3)}$ band is often considered as the obvious evidence of the ordered structure ($P4_332$) of the spinel. Meanwhile, the strong bands around 402, 239, 218 and 161 cm^{-1} are also the features of $P4_332$ structure. Therefore, it can be seen from Fig. 2b that the non-doped $LiNi_{0.5}Mn_{1.5}O_4$ has the characteristics of $P4_332$ structure. With increasing the Al content, the intensity of all these bands gradually lowers. when $2x \ge 0.20$, the bands around 402, 239, 218 and 161 cm^{-1} almost disappear; only three broadened bands exist at around 494, 603 and 638 cm^{-1}. These results indicate that the introduction of Al increases the disordering degree in the B-sites of the spinel. According to Strobel et al.'s study [33], the main driving force for such an octahedral cation ordering in $Li_2Mn_3MO_8$ is the charge difference between Mn and M atoms. Therefore, in the $LiNi_{0.5-x}Al_{2x}Mn_{1.5-x}O_4$, with increasing Al^{3+} content, the charge difference between Mn and M (Ni and Al) decreases, so that the cation ordering degree also decreases.

Fig. 3 shows the scanning electron microscopy (SEM) images of the $LiNi_{0.5-x}Al_{2x}Mn_{1.5-x}O_4$ ($0 \le 2x \le 1.0$) powders. It can be found that the particle morphologies of the samples are almost the same when $2x \le 0.2$. The well-identified octahedral morphologies suggest that the samples are all well crystallized spinels. However, when the content of Al ($2x$) exceeds 0.6, the particle morphologies are completely different. Severe aggregations of irregular-shaped nanoparticles can be observed.

3.2. Electrochemical characterization

Fig. 4a–g shows the 2nd cyclic voltammograms of the Li/$LiNi_{0.5-x}Al_{2x}Mn_{1.5-x}O_4$ ($0 \le 2x \le 0.6$) cells. On both cathodic and anodic runs, two peaks are observed at around 4.6–4.8 V, corresponding to the redox reactions of Ni^{2+}/Ni^{3+} and Ni^{3+}/Ni^{4+}. It is interesting to notice that the discrepancy between these two peaks has a clear relationship with the Al content. The voltage differences (ΔV) between these two peaks are plotted with $2x$ in Fig. 4h. Obviously, ΔV increases with $2x$, and a leap from ~30 mV to ~60 mV is observed at $2x = 0.075$. Kim et al. have shown that the voltage difference in the $Fd\bar{3}m$ type $LiNi_{0.5}Mn_{1.5}O_4$ is greater than that in the $P4_332$ type [1]. So we can conclude that ΔV is affected by the disordering degree of cations, higher disordering degree lead to larger ΔV. Note that, another peak at around 4.1 V is due to Mn^{3+}/Mn^{4+} redox couple. From the intensity of the peak we can conclude that the content of Mn^{3+} in the $LiNi_{0.5-x}Al_{2x}Mn_{1.5-x}O_4$ increases

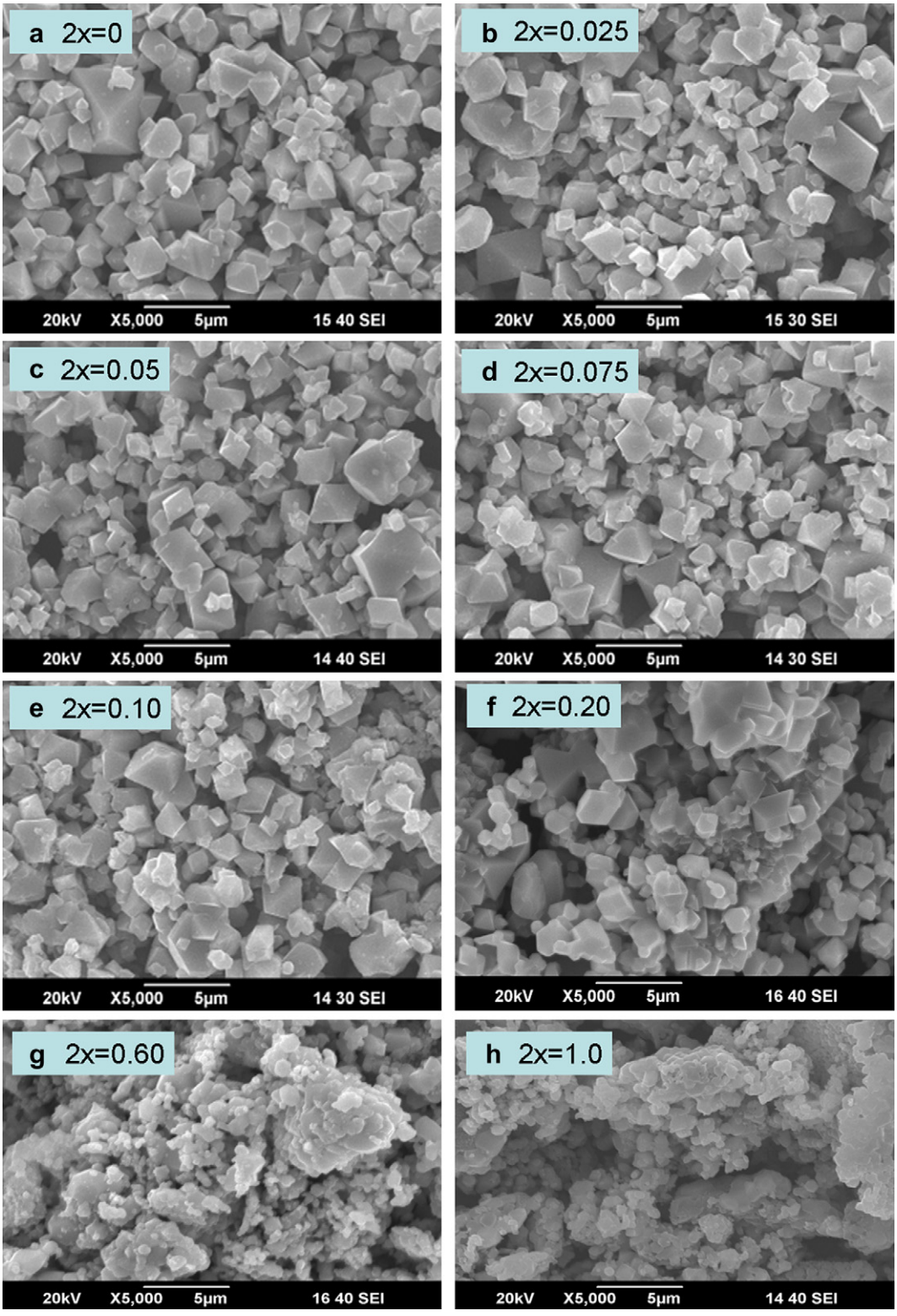

Fig. 3. SEM images of $LiNi_{0.5-x}Al_{2x}Mn_{1.5-x}O_4$ ($0 \leq 2x \leq 1.0$) powders.

with increasing the Al concentration in the spinel. We can roughly calculate the amount of Mn^{3+} to be 0.03, 0.05, 0.05, 0.07, 0.07, 0.09 and 0.17 in a unit formula of $LiNi_{0.5-x}Al_{2x}Mn_{1.5-x}O_4$ with $2x = 0$, 0.025, 0.05, 0.075, 0.10, 0.20 and 0.60, respectively.

The electrochemical cycling stabilities of the samples at room temperature and 55 °C are tested by galvanostatically charging/discharging the cells $Li/LiNi_{0.5-x}Al_{2x}Mn_{1.5-x}O_4$ ($0 \leq 2x \leq 0.6$) at 1C rate (the C rate is calculated based on their reversible capacity at low current density). The cycle performance at room temperature and 55 °C are showed in Fig. 5. Their charge/discharge curves of the 1st, 100th, 200th, 300th, 400th, and 500th cycles at room temperature are presented in Fig. 6. Their initial capacities and capacity retention along with their theoretical capacities are listed in Table 1. With increasing the Al content, the theoretical capacity of

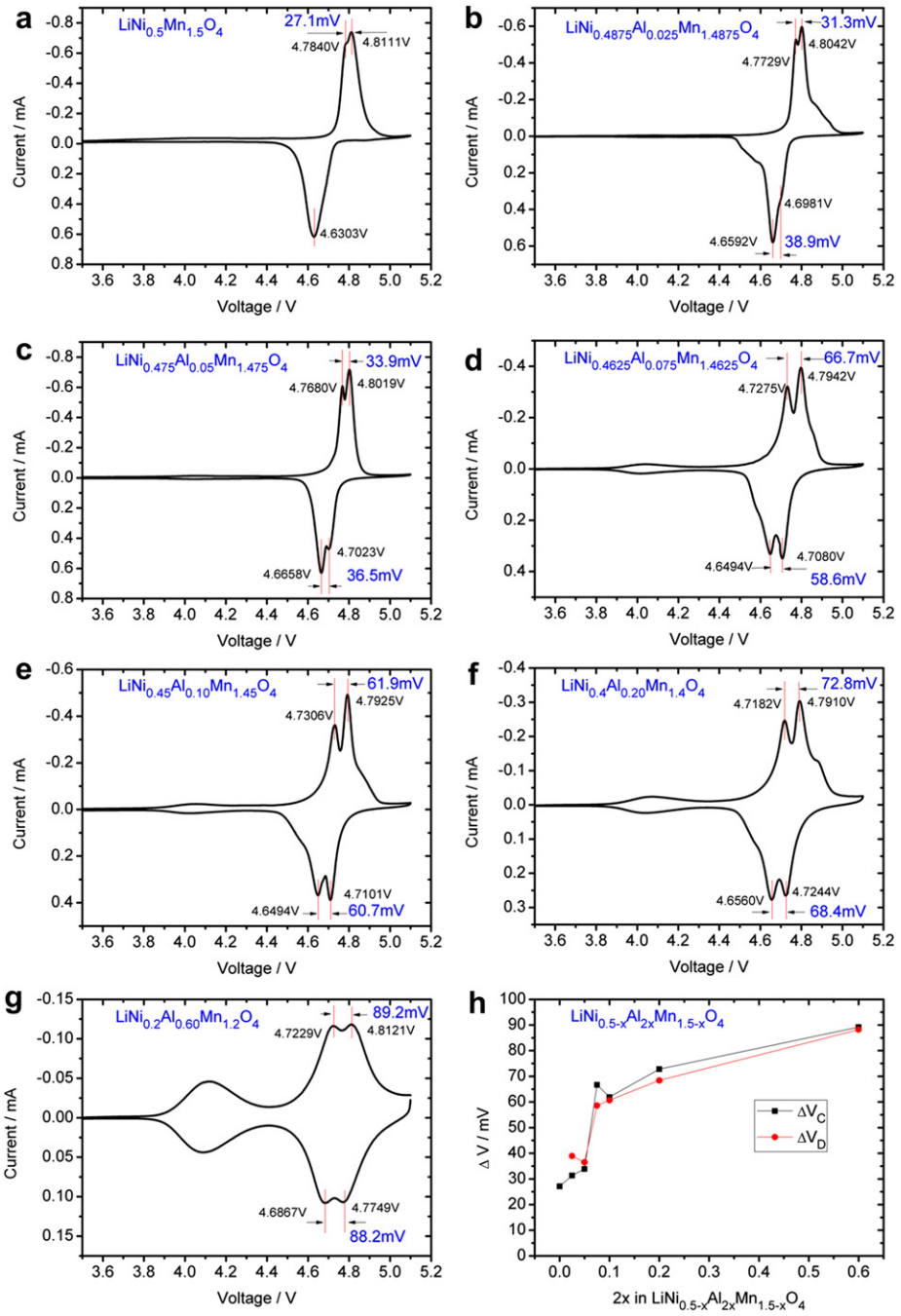

Fig. 4. (a–g) Cyclic voltammograms of $LiNi_{0.5-x}Al_{2x}Mn_{1.5-x}O_4$ ($0 \le 2x \le 0.6$) powders; (h) Relationship between the change of the voltage step (ΔV) between redox reactions Ni^{2+}/Ni^{3+} and Ni^{3+}/Ni^{4+} and the Al content ($2x$).

the $LiNi_{0.5-x}Al_{2x}Mn_{1.5-x}O_4$ spinels decreases because Al^{3+} ions are electrochemically inert. However, the reductions in the initial capacity are very small when the Al content is in the range of $0 \le 2x \le 0.1$. For higher doping ($2x \ge 0.2$), the initial capacities of the $LiNi_{0.5-x}Al_{2x}Mn_{1.5-x}O_4$ spinels further decrease, but they are very close to or even exceed their theoretical capacities. This is attributed to the compensation effect of Mn^{3+} ions in the spinels. With the $LiNi_{0.2}Al_{0.6}Mn_{1.2}O_4$ for example, the capacity at the 4.0 V plateau is 27.2 mAh g^{-1}, about 42% of its theoretical capacity (Fig. 6g). This additional contribution of capacity can cause the measured reversible capacity of a $LiNi_{0.2}Al_{0.6}Mn_{1.2}O_4$ to be much higher than its theoretical capacity predicted only by the 4.7 V plateau. The measured capacity at 4.0 V (27.2 mAh g^{-1}) suggests that there is a substantial amount of Mn^{3+} present in the sample. To maintain charge neutrality, we may consider the possible existence of oxygen vacancy in the structure to have a real composition of $LiNi_{0.2}Al_{0.6}Mn(III)_{0.168}Mn(IV)_{1.032}O_{3.916}$.

In fact, the case of $LiAlMnO_4$ has been reported by LeCras et al. [34]. It is electrochemically inactive as a cathode material, but it is active as an anode material. For the latter, it can change to Li_2AlMnO_4 by intercalating 1 mol lithium ions, delivering a theoretical capacity of 175 mAh g^{-1} with two voltage plateaus located at about 2.8 and 2.0 V. However, the cycle performance of $LiAlMnO_4$ as an anode material is poor and not shown here.

The pristine $LiNi_{0.5}Mn_{1.5}O_4$ delivers an initial discharge capacity of 133.0 mAh g^{-1} at room temperature. But with increasing the

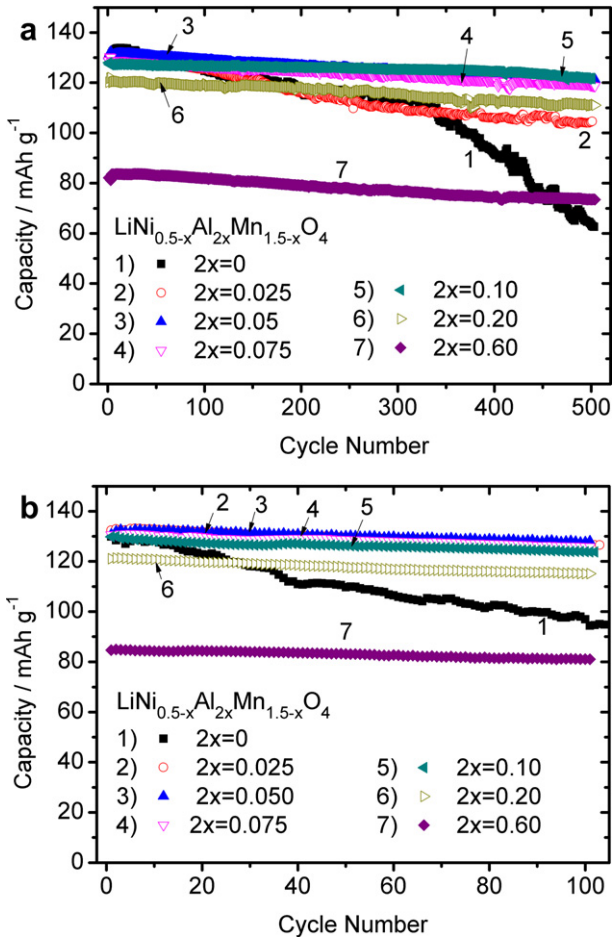

Fig. 5. Cyclic performance of Li/$LiNi_{0.5-x}Al_{2x}Mn_{1.5-x}O_4$ ($0 \le 2x \le 0.6$) cells at (a) room temperature and (b) 55 °C. The cells were charged/discharged at 1C rate.

cycle number, it suffers from significant polarization increase and severe capacity fading (Fig. 6a). Only a capacity of 63.0 mAh g^{-1} is measured at the 500th cycle with the capacity retention of 47%, and almost half of the capacity is from the 5 V constant-voltage process. Remarkably, the cycle performance of the spinel is significantly improved by Al-doping. The polarization is effectively suppressed for the sample $2x = 0.025$, the capacity retention of which also increases to 79.9% after 500 cycles. When the Al concentration increases to $2x \ge 0.05$, the polarization is very small, and the capacity retention further increases to over 92%, with a maximum capacity retention of 95.4% when $2x = 0.10$. Moreover, it can be seen from the curves that almost no change occurs for the 4.0 V plateau during cycling (Fig. 6a–g). Furthermore, the cycle performance at elevated temperature is also dramatically improved due to the doping of Al ions (Fig. 5b). The capacity retention after 100 cycles increases from 74.7% for $LiNi_{0.5}Mn_{1.5}O_4$ to over 95% for the samples with $0.025 \le 2x \le 0.6$.

The improved electrochemical properties can be partly attributed to the change of the structure from $P4_332$ to $Fd\bar{3}m$ because it has been confirmed that, even for the non-doped $LiNi_{0.5}Mn_{1.5}O_4$ cathode, the symmetry of $Fd\bar{3}m$ helps to have better electrochemical performance than the $P4_332$ symmetry structure [1]. On the other hand, because the Gibbs energy of the formation of NiO, Mn_2O_4 and Al_2O_3 is −211.7, −465.2 and −1576.4 kJ mol^{-1}, respectively, the bonding strength between the transition metal elements and oxygen can be strengthened by the incorporation of trivalent Al in the structure. Thus, the excellent cycling property of Al-doped $LiNi_{0.5-x}Al_{2x}Mn_{1.5-x}O_4$ may be also attributed to the reinforced crystal structure.

To investigate the effect of Al concentration on the rate capability, the cells Li/$LiNi_{0.5-x}Al_{2x}Mn_{1.5-x}O_4$ ($0 \le 2x \le 0.1$) are galvanostatically charged at room temperature at 0.5C rate and discharged under different current densities from 0.5C to 10C rate and then back to 0.5C. The discharge capacity values at various C-rates are plotted in Fig. 7. With increasing the current density, the Al-free $LiNi_{0.5}Mn_{1.5}O_4$ exhibits a gradual decrease in capacity. At 10C rate, the obtained capacity is only around 45 mAh g^{-1}. In contrast, the rate property is significantly improved even by doping with a small amount of Al. Over 85% of their capacities at 0.5C rate are retained at 10C rate for $LiNi_{0.5-x}Al_{2x}Mn_{1.5-x}O_4$ spinels ($0.025 \le 2x \le 0.10$). Among them, $LiNi_{0.45}Al_{0.10}Mn_{1.45}O_4$ demonstrates the best rate performance because a reversible capacity of 119 mAh g^{-1} is maintained at 10C rate, about 93.7% of its discharge capacity at 0.5C rate.

For the above optimized composition $LiNi_{0.45}Al_{0.10}Mn_{1.45}O_4$, we further investigate its prolonged cyclic stability at different charge/discharge rates and elevated temperature (Fig. 8). The tag "1C5D@RT" means that the cell is charged at 1C rate and discharged at 5C rate at room temperature; other tags have similar meanings. It can be seen that with increasing the discharge rate, the cells suffer aggravated capacity fading. When the cell is discharged at 10C at room temperature ("1C10D"), the capacity decreases substantially from 117 to only 3 mAh g^{-1} after 500 cycles. However, the $LiNi_{0.45}Al_{0.10}Mn_{1.45}O_4$ demonstrates quite good stability at a lower rate of 5C ("1C5D"), even if charged at the same rate ("5C5D"). For the "5C5D@RT" conditions, its reversible capacity decreases from 122 to 109 mAh g^{-1} in 150 cycles, while the fading becomes slower after 150-cycle in that only 5 mAh g^{-1} is reduced in the following 350 cycles. The $LiNi_{0.45}Al_{0.10}Mn_{1.45}O_4$ also presents good cyclic stability at 55 °C under the conditions of "1C1D". A capacity of 111 mAh g^{-1} is maintained after 500 cycles with the capacity retention of 86.0%.

3.3. Thermal stability

Safety concern is always one of the most important issues for the development of lithium-ion batteries, especially for the high voltage cathode $LiNi_{0.5}Mn_{1.5}O_4$. Xiang et al. have investigated the thermal stability of a $LiPF_6$-based electrolyte in contact with various delithiated cathodes of Li-ion batteries by C80 calorimetry [7]. Here the same method is adopted to examine the thermal property of the Al-doped spinels. Fig. 9 shows the heat flow curves of delithiated $LiNi_{0.5-x}Al_{2x}Mn_{1.5-x}O_4$ ($2x = 0$, 0.05, 0.10 and 0.20) in contact with a $LiPF_6$-based electrolyte. For $LiNi_{0.5}Mn_{1.5}O_4$, three main exothermic peaks appear at the positions of 108 °C, 145 °C and 246 °C. According to Xiang et al., the peaks below 225 °C are affected directly by reactions between the cathode materials and electrolyte, while the peak above 225 °C is attributed to decomposition of the products obtained earlier. In Fig. 9, the onset temperature of the third peak for all samples is about 220 °C, and there is no obvious change for the intensity of this peak. However, the other two peaks below 220 °C are successfully suppressed by Al-doping. The $LiNi_{0.5}Mn_{1.5}O_4$ system has the highest reaction heat flow of 301 J g^{-1} in the temperature range of 50–225 °C. It can be found easily that the intensity of the peaks at 108 °C and 145 °C are gradually weakened with increasing Al concentration. For the $LiNi_{0.4}Al_{0.2}Mn_{1.4}O_4$, the total heat flow generated in the same temperature range decreases to 139 J g^{-1}. Because the thermal runaway of the battery mostly occurs below 200 °C, so the reaction heat released below 220 °C is considered as one of the most important indicator for evaluating the thermal stability of lithium-ion batteries. In this regard, Al-doping is an effective way to improve the safety of the $LiNi_{0.5}Mn_{1.5}O_4$.

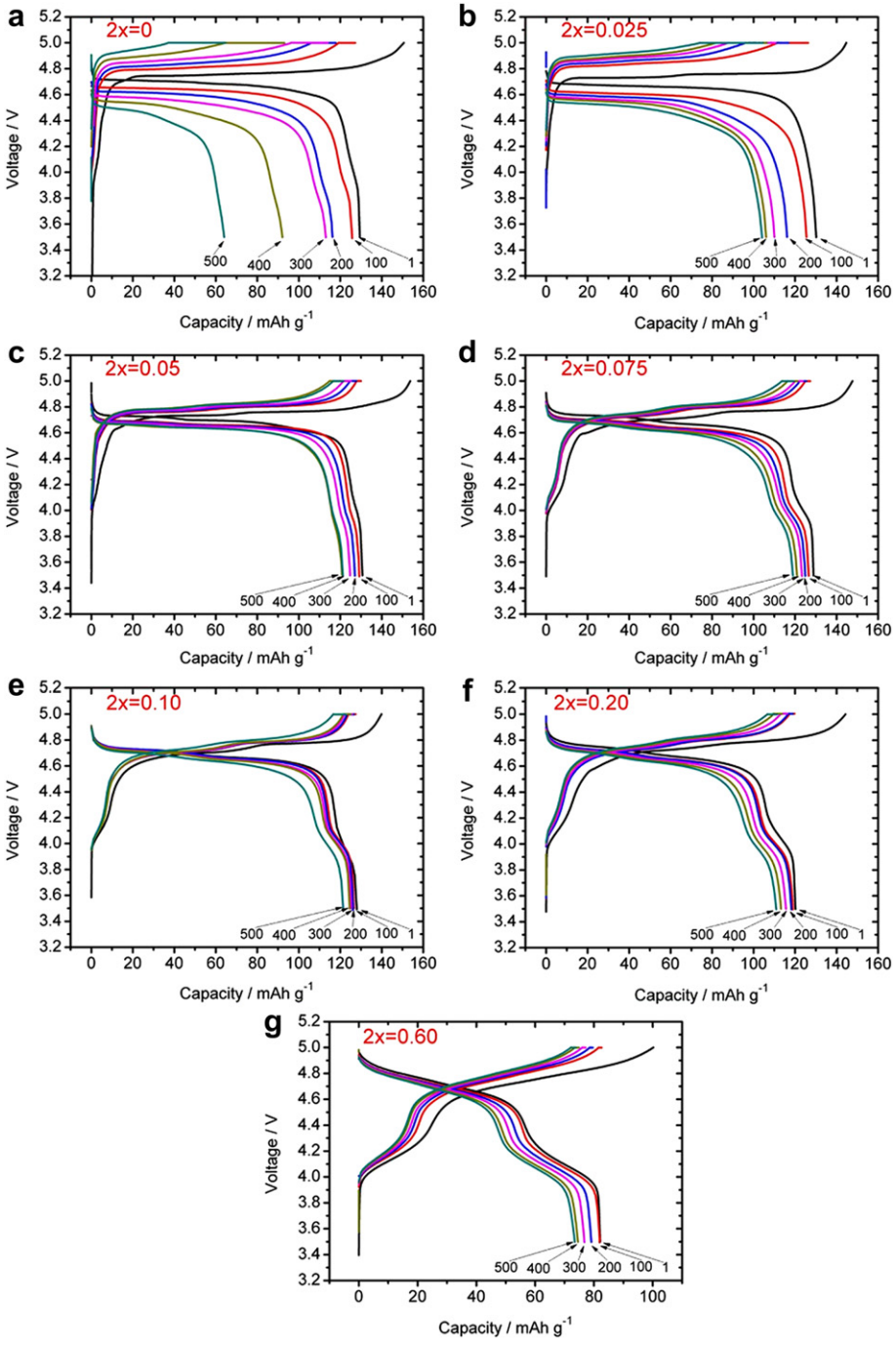

Fig. 6. The charge/discharge curves of the $LiNi_{0.5-x}Al_{2x}Mn_{1.5-x}O_4$ ($0 \leq 2x \leq 0.6$) samples at the 1st, 100th, 200th, 300th, 400th, and 500th cycles at room temperature.

Table 1
The theoretical capacity, the initial capacity and capacity retention of the $LiNi_{0.5-x}Al_{2x}Mn_{1.5-x}O_4$ ($0 \leq 2x \leq 0.6$) at room temperature and 55 °C.

		RT			55 °C		
$2x$	Theoretical capacity (mAh g^{-1})	Initial discharge capacity (mAh g^{-1})	500th discharge capacity (mAh g^{-1})	Capacity retention (%)	Initial discharge capacity (mAh g^{-1})	100th discharge capacity (mAh g^{-1})	Capacity retention (%)
0	146.7	133.0	63.0	47.4	129.9	97.0	74.7
0.025	143.6	130.8	104.5	79.9	132.4	126.7	95.7
0.05	140.5	130.5	121.4	93.0	130.8	127.8	97.7
0.075	137.4	128.4	118.7	92.4	130.6	126.0	96.5
0.10	134.3	127.4	121.6	95.4	129.9	123.9	95.4
0.20	121.3	120.1	111.3	92.7	121.1	115.1	95.0
0.60	65.1	83.5	73.5	88.0	84.6	81.1	95.9

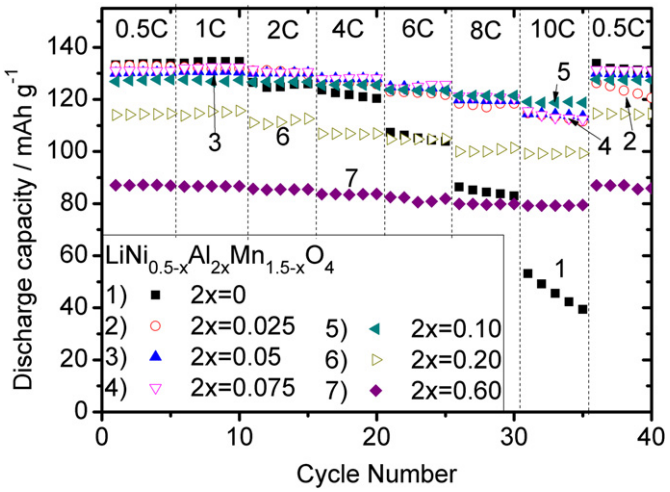

Fig. 7. Discharge capacity values of Li/$LiNi_{0.5-x}Al_{2x}Mn_{1.5-x}O_4$ ($0 \le 2x \le 0.6$) cells at various C-rates from 0.5C to 10C. The doped spinels exhibit significantly improved rate performance compared with the undoped $LiNi_{0.5}Mn_{1.5}O_4$.

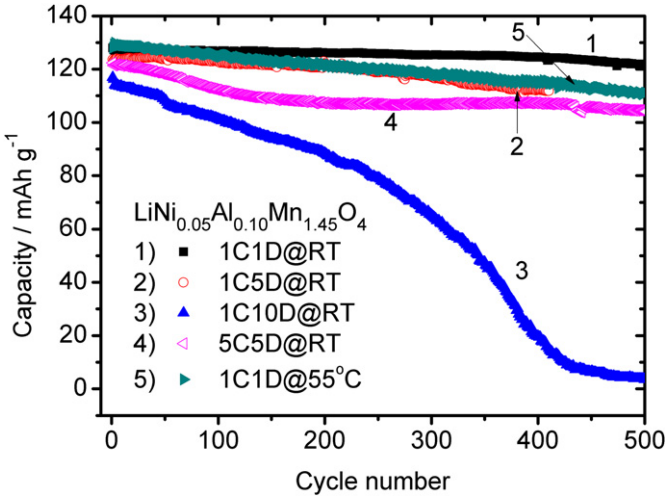

Fig. 8. The prolonged cyclic performance of Li/$LiNi_{0.45}Al_{0.10}Mn_{1.45}O_4$ cells at different charge/discharge rates at room temperature and at 55 °C.

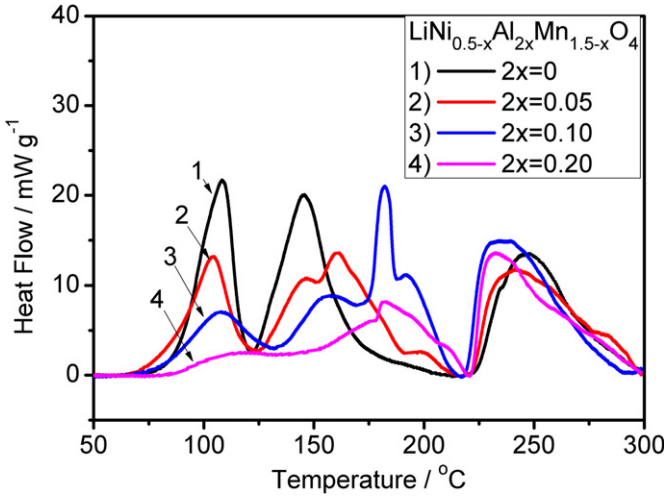

Fig. 9. C80 heat flow curves of coexistence systems of 20 mg delithiated cathode materials ($LiNi_{0.5-x}Al_{2x}Mn_{1.5-x}O_4$ with $2x = 0$, 0.05, 0.10 and 0.20) and 50 mg electrolyte (1 M $LiPF_6$/EC + DMC) at a heating rate of 0.2 °C min^{-1}.

4. Conclusions

A series of Al-doped $LiNi_{0.5-x}Al_{2x}Mn_{1.5-x}O_4$ ($0 \le 2x \le 1.0$) spinel powders have been synthesized by a thermopolymerization method. The effects of Al-doping on the structural, electrochemical and thermal properties of the spinels have been investigated. The solid solubility of Al in $LiNi_{0.5-x}Al_{2x}Mn_{1.5-x}O_4$ is less than 0.6. The introductions of Al in the lattice favor the change of the space group of $LiNi_{0.5}Mn_{1.5}O_4$ from ordered $P4_332$ to disordered $Fd\bar{3}m$. The cyclic stability and rate property are significantly improved by Al-doping without obvious capacity reduction in the optimized Al concentration of $0.05 \le 2x \le 0.10$. The $LiNi_{0.45}Al_{0.10}Mn_{1.45}O_4$ gives the best capacity retention (95.4% after 500 cycles at 1C rate) and the best rate capability (119 mAh g^{-1} at 10C, about 93.7% of its capacity at 0.5C) at room temperature. The Al-doping can also dramatically suppress the exothermic reaction below 220 °C, thus improve the safety of the high voltage cathode material.

Acknowledgments

This study was supported by National Science Foundation of China (grant nos. 20971117, 10979049 and J1030412) and Education Department of Anhui Province (grant no. KJ2009A142). We are also grateful to the Solar Energy Operation Plan of Academia Sinica.

References

[1] J.H. Kim, S.T. Myung, C.S. Yoon, S.G. Kang, Y.K. Sun, Chem. Mater. 16 (2004) 906.
[2] K. Ariyoshi, Y. Iwakoshi, N. Nakayama, T. Ohzuku, J. Electrochem. Soc. 151 (2004) A296.
[3] K.M. Shaju, P.G. Bruce, Dalton Trans. (2008) 5471.
[4] G.B. Zhong, Y.Y. Wang, Z.C. Zhang, C.H. Chen, Electrochim. Acta 56 (2011) 6554.
[5] J.-M. Tarascon, Phil. Trans. R. Soc. 368 (2011) 3227.
[6] R. Marom, S.F. Amalraj, N. Leifer, D. Jacob, D. Aurbach, J. Mater. Chem. 21 (2011) 9938.
[7] H.F. Xiang, H. Wang, C.H. Chen, X.W. Ge, S. Guo, J.H. Sun, W.Q. Hu, J. Power Sources 191 (2009) 575.
[8] Y.E. Hyung, D.R. Vissers, K. Amine, J. Power Sources 119 (2003) 383.
[9] K. Xu, S.S. Zhang, J.L. Allen, T.R. Jow, J. Electrochem. Soc. 149 (2002) A1079.
[10] H.F. Xiang, H.Y. Xu, Z.Z. Wang, C.H. Chen, J. Power Sources 173 (2007) 562.
[11] H.F. Xiang, Q.Y. Jin, C.H. Chen, X.W. Ge, S. Guo, J.H. Sun, J. Power Sources 174 (2007) 335.
[12] S.S. Zhang, J. Power Sources 162 (2006) 1379.
[13] J.A. Choi, Y.K. Sun, E.G. Shim, B. Scrosati, D.W. Kim, Electrochim. Acta 56 (2011) 10179.
[14] H. Sakaebe, H. Matsumoto, K. Tatsumi, Electrochim. Acta 53 (2007) 1048.
[15] M. Armand, F. Endres, D.R. MacFarlane, H. Ohno, B. Scrosati, Nat. Mater. 8 (2009) 621.
[16] A. Lewandowski, A. Swiderska-Mocek, J. Power Sources 194 (2009) 601.
[17] A. Balducci, S.S. Jeong, G.T. Kim, S. Passerini, M. Winter, M. Schmuck, G.B. Appetecchi, R. Marcilla, D. Mecerreyes, V. Barsukov, V. Khomenko, I. Cantero, I. De Meatza, M. Holzapfel, N. Tran, J. Power Sources 196 (2011) 9719.
[18] H.L. Wang, H. Xia, M.O. Lai, L. Lu, Electrochem. Commun. 11 (2009) 1539.
[19] T.A. Arunkumar, A. Manthiram, Electrochim. Acta 50 (2005) 5568.
[20] D.Q. Liu, Y.H. Lu, J.B. Goodenough, J. Electrochem. Soc. 157 (2010) A1269.
[21] J. Liu, A. Manthiram, J. Electrochem. Soc. 156 (2009) A66.
[22] J. Liu, A. Manthiram, J. Phys. Chem. C 113 (2009) 15073.
[23] Y.K. Sun, K.J. Hong, J. Prakash, K. Amine, Electrochem. Commun. 4 (2002) 344.
[24] Y.K. Sun, C.S. Yoon, I.H. Oh, Electrochim. Acta 48 (2003) 503.
[25] J.S. Kim, C.S. Johnson, J.T. Vaughey, S.A. Hackney, K.A. Walz, W.A. Zeltner, M.A. Anderson, M.M. Thackeray, J. Electrochem. Soc. 151 (2004) A1755.
[26] J. Liu, A. Manthiram, Chem. Mater. 21 (2009) 1695.
[27] J.C. Arrebola, A. Caballero, L. Hernan, J. Morales, Eur. J. Inorg. Chem. (2008) 3295.
[28] U. Lafont, C. Locati, W.J.H. Borghols, A. Lasinska, J. Dygas, A.V. Chadwick, E.M. Kelder, J. Power Sources 189 (2009) 179.
[29] M. Kunduraci, G.G. Amatucci, J. Electrochem. Soc. 153 (2006) A1345.
[30] M. Kunduraci, J.F. Al-Sharab, G.G. Amatucci, Chem. Mater. 18 (2006) 3585.
[31] S.H. Oh, K.Y. Chung, S.H. Jeon, C.S. Kim, W.I. Cho, B.W. Cho, J. Alloy Compd. 469 (2009) 244.
[32] C.M. Julien, M. Massot, Mat. Sci. Eng. B-Solid 97 (2003) 217.
[33] P. Strobel, A. Ibarra-Palos, M. Anne, C. Poinsignon, A. Crisci, Solid State Sci. 5 (2003) 1009.
[34] F. LeCras, D. Bloch, M. Anne, P. Strobel, Solid State Ionics 89 (1996) 203.